# High-Pressure Effects on the Electronic Structure of Anthracene Single Crystals: Role of Nonhydrostaticity

**ARTICLE** *in* THE JOURNAL OF PHYSICAL CHEMISTRY A · FEBRUARY 2009

Impact Factor: 2.69 · DOI: 10.1021/jp808247k · Source: PubMed



**4 AUTHORS**, INCLUDING:

Zbigniew Dreger
Washington State University
**124** PUBLICATIONS **1,126** CITATIONS

SEE PROFILE

THE JOURNAL OF PHYSICAL CHEMISTRY A



Article

# High-Pressure Effects on the Electronic Structure of Anthracene Single Crystals: Role of Nonhydrostaticity

Z. A. Dreger, E. Balasubramaniam, Y. M. Gupta, and A. G. Joly

*J. Phys. Chem. A*, **2009**, 113 (8), 1489-1496• DOI: 10.1021/jp808247k • Publication Date (Web): 22 January 2009

# High-Pressure Effects on the Electronic Structure of Anthracene Single Crystals: Role of Nonhydrostaticity

**Z. A. Dreger,* E. Balasubramaniam, and Y. M. Gupta**

*Institute for Shock Physics, Washington State University, Pullman, Washington 99164*

**A. G. Joly**

*Pacific Northwestern National Laboratory, Richland, Washington 99352*

*Received: September 16, 2008; Revised Manuscript Received: December 4, 2008*

Optical spectroscopy methods were used to examine the effect of nonhydrostaticity on the electronic structure of anthracene single crystals compressed statically to 9 GPa. Two pressure-transmitting media, nitrogen (hydrostatic) and water (nonhydrostatic above ~5.5 GPa), were utilized. It was found that nonhydrostatic compression generates several new features both in the absorption and fluorescence spectra: (i) formation of new absorption and fluorescence bands, (ii) deviations in pressure shift of fluorescence peaks, (iii) extensive broadening of vibrational peaks, and (iv) irreversible changes in the spectra shape upon pressure unloading. Furthermore, the time-resolved fluorescence decay curves measured at the wavelength corresponding to the new fluorescence band show clear initial increase. These new features are accompanied by inhomogeneous color changes and macroscopic lines on the (001) plane of the crystal. All of the changes are discussed and correlated with microscopic transformations in the crystal. It is demonstrated that nonhydrostatic compression in anthracene crystal introduces inelastic changes in the form of dislocations along [110] and [1$\bar{1}$0] directions. These dislocations lead to the development of dimeric structures and, consequently, to various changes in the electronic response of the compressed anthracene crystal.

## 1. Introduction

Due to relatively weak intermolecular interactions, molecular solids are very responsive to applied pressure. As such, pressure is a useful variable for altering and clarifying structure−property relationship in these solids. Additionally, because of low symmetries and low elastic limits, pressure effects in molecular crystals are sensitive to loading conditions including nonhydrostaticity. Nonhydrostatic stresses can significantly change the response of molecular crystals and result in effects not observed otherwise under hydrostatic pressure. However, these effects are not well recognized and are often underestimated in studies on molecular crystals. Consequently, examination of nonhydrostatic effects is central to a proper understanding of physical and chemical processes in compressed molecular crystals.

Here, we present the results of a study on statically compressed anthracene single crystals ($C_{14}H_{10}$, and a crystal structure of $P2_1/a$). Anthracene—a polycyclic aromatic hydrocarbon and one of the most extensively studied organic molecular crystals—can be considered a prototype for this class of crystals. The interest in anthracene was stimulated mainly by its attractive electronic and optical properties and by advances in its purification and crystal growth.[1−3] Pressure effects on the crystal and electronic structures of anthracene have attracted considerable attention in the past.[4−18] Despite extensive studies, results reported from different laboratories have varied significantly. For example, some changes in vibrational and electronic spectra were observed at pressures around (1−2) GPa. They were frequently attributed either to a second-order phase transition[6,12,14,20,21] or an excimer-like fluorescence.[5,8,10,13] Recently, it was recognized that the observed changes depend strongly on the pressure-transmitting medium surrounding the anthracene sample.[13,19] Furthermore, it has been suggested that the onset of various changes in the crystal and electronic structures can be initiated by nonhydrostaticity.[13] However, a detailed characterization and understanding of these changes has not been provided to date.

The effect of nonhydrostaticity (and the resulting nonuniform stresses) on the electronic spectra of anthracene single crystals are presented here. To better understand the changes in electronic spectra, we complement these results with time-resolved fluorescence decay and optical imaging measurements. The use of these different methods provides a comprehensive approach and makes it possible to relate electronic changes to microscopic transformations in the crystal.

Specifically, we focus on the following questions. What features in the electronic spectra are associated with nonhydrostatic compression? How do these features correspond to changes in the electronic and crystal structures? What microscopic mechanism governs these changes? Answers to these questions will improve our understanding of the physical and chemical processes in nonhydrostatically compressed molecular crystals and should contribute to our broader understanding of the processes in compressed molecular systems.

The remainder of this paper is organized as follows. The next section describes the experimental methods. Experimental results are presented and discussed in section 3. Section 4 contains the concluding remarks from this work.

## 2. Experimental Methods

**2.1. Sample Preparation and High-Pressure Generation.** Solution-grown anthracene single crystals were used in this study. Zone-refined, 99.9% pure anthracene was purchased from

* Corresponding author. E-mail: dreger@wsu.edu.

10.1021/jp808247k CCC: $40.75 
Published on Web 01/22/2009

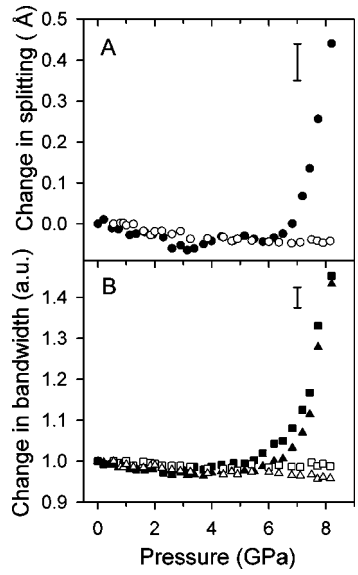


**Figure 1.** Pressure effects on the ruby $R_1$ and $R_2$ fluorescence lines in different media: nitrogen, open symbols; water, solid symbols. (A) Relative change in the ($R_1-R_2$) splitting. (B) Fluorescence peak bandwidths normalized to the 1 atm value: triangle and square symbols stand for the $R_1$ and $R_2$ lines, respectively. The bars in the top right corner of the graphs represent the detection resolution.

Aldrich. Single crystals were obtained from anthracene/dichloroethane solution by a slow cooling of the solvent.[3] The larger crystals, with thickness ~0.01−0.02 mm, were cut to approximate lateral dimensions of 0.08−0.15 mm$^2$. A diamond anvil cell (DAC) with low-fluorescence type II diamonds (0.06 mm culet size) was used for generating high pressures. A preindented stainless steel gasket with 0.2 mm aperture and 0.1 mm of height was used as the sample compartment. An anthracene single crystal oriented on the (001) plane, a ruby chip, and the pressure-transmitting medium filled the entire volume of the sample compartment. Pressure was calibrated using shifts of the ruby fluorescence lines. The ruby fluorescence was excited with a 532 nm ($18.8 \times 10^3$ cm$^{-1}$) CW diode-pumped laser.

Hydrostaticity/nonhydrostaticity of the pressure medium, in the DAC, was monitored by measuring the splitting changes between the $R_1$ and $R_2$ lines and by their bandwidths. Two different media nitrogen and water were utilized to provide hydrostatic and nonhydrostatic compressions. In Figure 1, we show pressure-induced changes in the splitting and the bandwidth of ruby lines in these two media. Cryogenically loaded nitrogen provided hydrostatic compression as evidenced by unchanged splitting and bandwidths of the $R_1$ and $R_2$ lines. Nonhydrostatic compression was generated using water. Water was selected because of its chemical inertness to anthracene. When water was used, a deviation from linearity in both the splitting and bandwidth of the ruby lines was clearly observed above ~5 GPa indicating the onset of nonhydrostaticity. Note that changes in the bandwidth occur at a slightly lower pressure than changes in the splitting. However, both of these changes occur at much higher pressures than the liquid−solid phase transition in water which occurs at ~1.0 GPa.

Although changes in splitting between the $R_1$ and $R_2$ lines and changes in their bandwidths are generally related in DAC experiments, they have a different physical basis. Shock compression studies of ruby R-lines have shown that the change in splitting is related to stress deviators and the change in the bandwidth is related to nonuniform stress or stress gradients.[22−24] Furthermore, the magnitude of the change in splitting depends on the relative orientation of the ruby crystals with respect to the imposed stress field.[22−24] To determine the pressure (mean stress) imposed on the crystal under nonhydrostatic compression, the $R_2$ line shift was employed because it is independent of the nonhydrostaticity.[22] We monitored both the splitting and bandwidth during the experiment to assess the stress conditions in the high-pressure cell. In water, the pressure gradients developed before the occurrence of measurable stresses deviators (see Figure 1).

**2.2. Spectroscopic and Optical Measurements.** Absorption spectra were measured using a Cary 50 spectrometer with a fiber-optics attachment, permitting a reduction of the incident beam size to ~0.3 mm. The dynamic range of our absorption measurements was ~2.0.

Emission from the sample was excited using the 337 nm ($29.7 \times 10^3$ cm$^{-1}$) line from a nitrogen laser. An average power of ~1 mW at 30 Hz was employed. Occasionally, the 514.5 nm ($19.4 \times 10^3$ cm$^{-1}$) line from an argon ion laser was used for excitation. The emission spectra were collected in a backscattering geometry and dispersed onto the monochromator, equipped with a 300 grooves/mm grating blazed at 500 nm. Liquid nitrogen cooled CCD was used for detection. The spectra, recorded from 380 to 800 nm [$(26.3-12.5) \times 10^3$ cm$^{-1}$], were obtained at ambient temperature. All recorded spectra were corrected for the spectral sensitivity of the detection system. The spectra were analyzed using the PeakFit software to locate the positions and bandwidths of the emission peaks.

Time-dependent fluorescence measurements were performed using excitations 360 nm ($27.8 \times 10^3$ cm$^{-1}$) and 532 nm ($18.8 \times 10^3$ cm$^{-1}$) wavelengths. The 532 nm line was the frequency-doubled output from a mode-locked Nd:YAG laser, whereas the 360 nm line was the frequency-doubled output from a dye laser pumped with a second harmonic of the Nd:YAG laser. In both cases, the pulse width was shorter than 80 ps at 76 MHz repetition rate. A time-correlated single-photon counting system (TCSPCS) with a microchannel plate photomultiplier (MCP-PMT) and multichannel analyzer (MCA) was used for detection and analysis of fluorescence decays.[25,26] The time resolution of the system was ~37.5 ps/channel. A monochromator with a bandwidth of ~20 nm was used to extract the selected wavelength of the emitted light.

Optical images of compressed anthracene crystals were obtained using an imaging camera equipped with video zooming optics, objective, and optical microscope. The camera provided a video resolution of 2 megapixels with a real-time viewing option. The images were acquired in transmitted light, using a 12× video zoom optics and a large working distance objective (20 mm) with a 50× magnification.

## 3. Results and Discussion

**3.1. Changes in Electronic Spectra.** In Figure 2, we present the pressure effects on fluorescence spectra of anthracene single crystals compressed using nitrogen and water. As mentioned above, nitrogen provides hydrostatic compression over the entire pressure range studied, whereas water does so only up to ~5 GPa. The 337 nm wavelength was used for excitation in both experiments shown in Figure 2. The power of the incident light was kept low to avoid any irreversible light-induced processes. Under hydrostatic compression, the spectra show a shift to lower energy (red shift) with some broadening of vibronic bands, which is typical for aromatic compounds.[27] Additionally, the global fluorescence intensity decreases gradually with increasing pressure.[13] Energies of the vibronic bands were obtained by

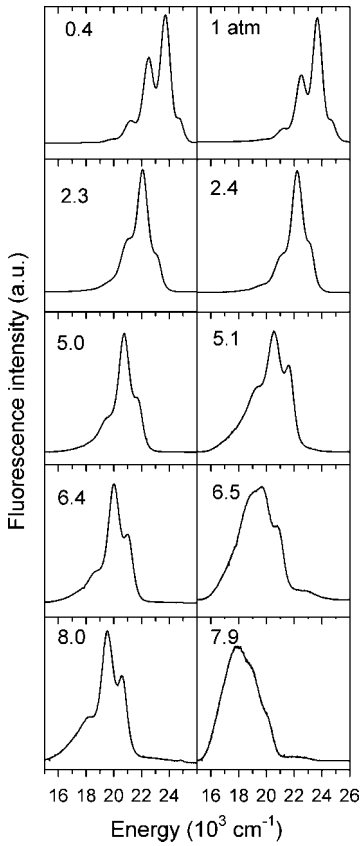


**Figure 2.** Fluorescence spectra of anthracene crystal at several pressures or mean stresses. The spectra displayed on the left are obtained in nitrogen which provides hydrostatic compression in this pressure range. The spectra displayed on the right are obtained in water which introduces nonhydrostatic compression above ~5 GPa. The numbers in panels represent pressure in GPa. The intensity is normalized to the maximum intensity of each spectrum. Spectra were corrected for instrumental sensitivity but not for the reabsorption effect.

fitting the fluorescence spectrum with the Gaussian−Lorentzian peaks. In the fitting procedure, the widths of the 0−1, 0−2, 0−3, and 0−4 vibronic bands for a given pressure were fixed at the same value. However, the 0−0 band assumed variable widths due to the reabsorption effect. More details and resulting values of fitting can be found elsewhere.[13]

In contrast, nonhydrostaticity that develops above 5 GPa introduces several new features in the spectra: (i) growth of the new low-energy band, (ii) larger shift of the spectrum to lower energies than under hydrostatic compression, (iii) broadening of vibronic bands that leads ultimately to a broad structureless spectrum, and (iv) larger decrease of fluorescence intensity than under hydrostatic compression. Some details of these changes are presented in Figures 3 and 4. As shown in Figure 3, the new low-energy band emerges already at 5.1 GPa with a peak located around 540 nm ($18.5 \times 10^3$ cm$^{-1}$). With increasing pressure, the intensity of this band increases and the position shifts to lower energies (Figure 4A). It is worth mentioning that the new emission band (NEB) remains in the spectrum upon release of the pressure; this implies irreversible changes in the crystal and is in contrast to the reversible changes under hydrostatic compression (see Figure 5). In addition, nonhydrostaticity affects the position and the bandwidth of vibronic bands. For instance, both the position and the bandwidth of the vibronic band corresponding to the 0−1 transition deviate from the values obtained under hydrostatic compression; that is, the bandwidth significantly increases and the peak shifts further to lower

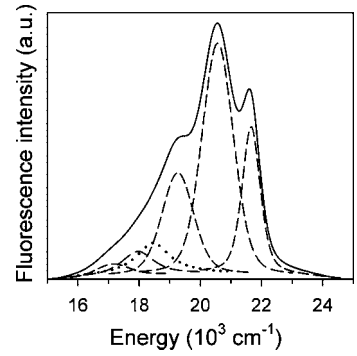


**Figure 3.** Example of deconvolution of the fluorescence spectrum into vibronic bands using the Gaussian−Lorentzian curves. All vibronic bands, except the 0−1 band, were fitted with the same width. The width of the 0−1 band was smaller due to the reabsorption effect. The spectrum was obtained at 5.1 GPa in water. The dotted line represents the band occurring at the onset of nonhydrostaticity.

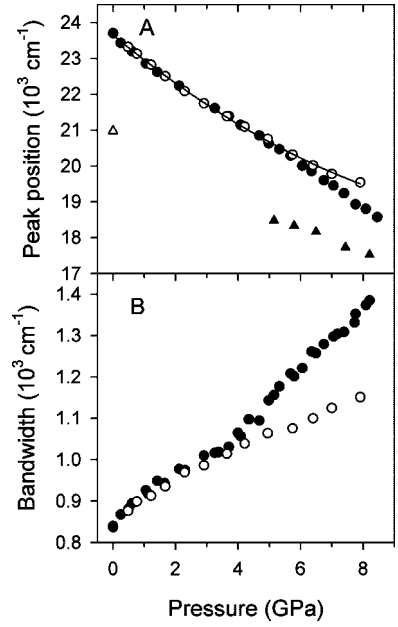


**Figure 4.** (A) Pressure effect on the position of the 0−1 vibronic band under hydrostatic (○) and nonhydrostatic compression (●). The solid line represents a polynomial fit to hydrostatic data (ref 13). The solid triangle (▲) represents a new low-energy band developed only under nonhydrostatic compression; this band is present in the spectrum upon pressure release, and the open triangle denotes the position of this band at ambient pressure. (B) Pressure effect on the bandwidth of the 0−1 vibronic band under hydrostatic (○) and nonhydrostatic compression (●).

energies (Figure 4). Bandwidth broadening can be associated with the increase in exciton−phonon interaction due to the reduction of intermolecular distances under pressure,[27] whereas extensive broadening can imply crystal deformation resulting from inhomogeneous stresses.[28] Furthermore, the larger pressure shift of vibronic bands could suggest a softening of the crystal microstructure under nonhydrostatic compression.

Development of a new band in the fluorescence spectra clearly indicates changes in the electronic structure, specifically, in the excited states. However, the absorption spectra also reveal changes at the onset of nonhydrostaticity. This result differs from previously reported results for polycrystalline samples, where only a pressure shift of the absorption edge was observed.[4] Figure 6 shows clearly that a new absorption band develops at the shoulder of the anthracene absorption edge above ~5 GPa, though this band dies out after release of the pressure.

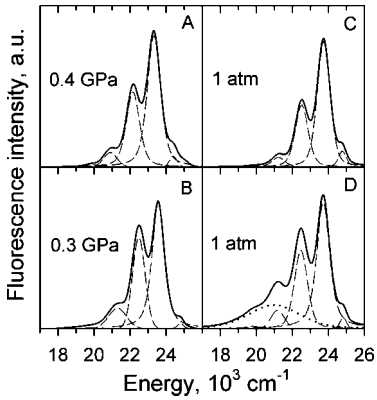


**Figure 5.** Changes in fluorescence spectra upon pressure release. (A and B) Spectra measured at nearly ambient pressure before and after hydrostatic compression to ~8 GPa; the lowest pressure with $N_2$ as a pressure-transmitting medium was 0.3−0.4 GPa. (C and D) Spectra measured at ambient pressure before and after nonhydrostatic compression to 8.3 GPa. Dashed lines denote the vibronic bands. The dotted line denotes the new emission band.

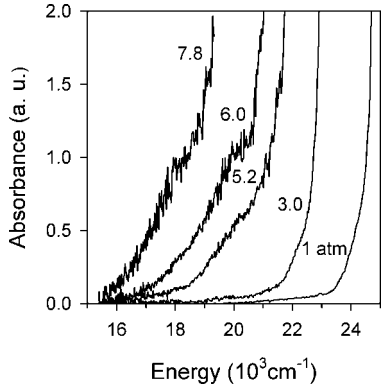


**Figure 6.** Pressure effect on absorption spectra (absorption edge) of anthracene single crystal. The spectra were measured in $H_2O$ as a pressure-transmitting medium; nonhydrostaticity was introduced above 5 GPa.

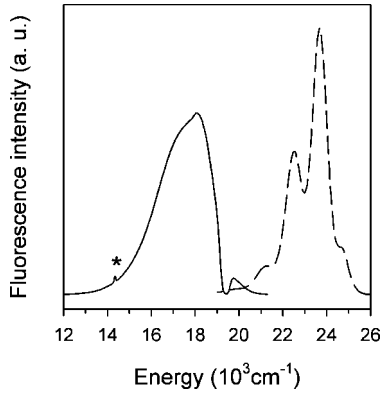


**Figure 7.** Fluorescence spectrum of anthracene under nonhydrostatic compression at 6 GPa (solid line). The spectrum was obtained with excitation of 514.5 nm ($19.4 \times 10^3$ cm$^{-1}$). The excitation line was separated from the spectrum with the use of notch filter. The asterisk denotes the fluorescence line from the ruby crystal. The ambient spectrum (dashed line) obtained with excitation of 337 nm ($29.7 \times 10^3$ cm$^{-1}$) wavelength is shown for comparison.

The association between the new absorption and fluorescence bands is examined with the excitation of the 514.5 nm ($19.4 \times 10^3$ cm$^{-1}$) line, which matches the energy of the new absorption band. As shown in Figure 7, this excitation leads to a broad and structureless fluorescence spectrum. The shape of this spectrum resembles to some extent the shape of the spectrum obtained with the 337 nm excitation line (see the graph at 7.9 GPa in Figure 2), implying the possibility of similar species being involved in the fluorescence spectra for these two excitation energies. This hypothesis is examined further with time-dependent fluorescence measurements.

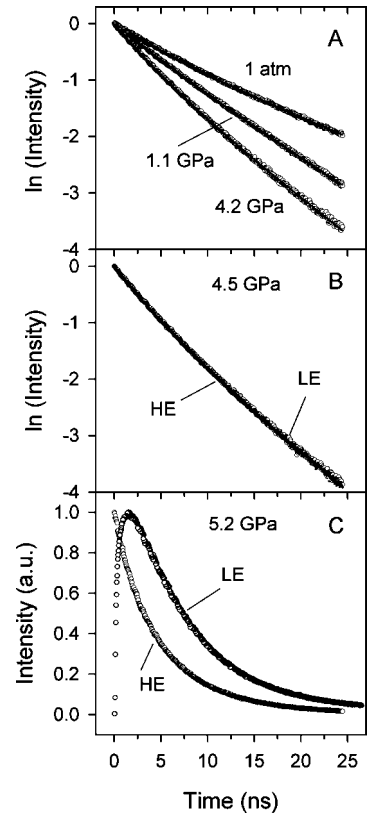


**Figure 8.** Fluorescence decay curves under hydrostatic and nonhydrostatic compressions upon excitation with the 360 nm ($27.8 \times 10^3$ cm$^{-1}$) line; points represent experimental data and solid lines represent fit using eq 1. (A) Fluorescence decays measured at the maximum fluorescence spectrum under hydrostatic compression for several pressures. (B) Fluorescence decays measured at the HE and LE parts of the fluorescence spectrum under hydrostatic compression of 4.5 GPa. (C) Fluorescence decays measured at the HE and LE parts of the fluorescence spectrum under nonhydrostatic compression of 5.2 GPa.

**3.2. Time-Resolved Fluorescence Decay Curves: Evidence for Formation of Structural Defects.** To gain insight into electronic structure changes of anthracene under nonhydrostatic compression, time-resolved fluorescence decay was measured following a picosecond laser excitation. Two sets of experiments were performed. In the first, excitation was accomplished using the 360 nm ($27.8 \times 10^3$ cm$^{-1}$) line and emission was measured at wavelengths related to the high- and low-energy part of the fluorescence spectrum. The use of 360 nm wavelength provided excitation of the anthracene singlet-exciton band. Monitoring the emission at different parts of spectra permitted examination of changes due to formation of the new emission band. The monitored wavelengths corresponding to the low-energy (LE) and high-energy (HE) parts of the spectrum were gradually increased as the fluorescence spectrum was shifting toward lower energies with increasing pressure. For instance, at 4.5 GPa these wavelengths were, respectively, 450 nm ($22.2 \times 10^3$ cm$^{-1}$) and 560 nm ($17.9 \times 10^3$ cm$^{-1}$). In the second set of experiments, a 532 nm wavelength was used for excitation and detection was performed at the wavelengths higher than 560 nm ($17.9 \times 10^3$

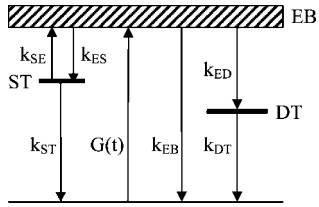


**Figure 9.** Energy level diagram for the kinetics of exciton migration in the presence of structural defects. $G(t)$ is the rate of singlet-excition creation. The EB, ST, and DT denote energy levels for the free excitons and those trapped in shallow and deep defects, respectively. $k_{EB}$, $k_{ST}$, and $k_{DT}$ are the decay rates from the above-mentioned levels; they contain the radiative and nonradiative contributions. $k_{ES}$ and $k_{ED}$ are the respective exciton transfer rates to shallow and deep defects. $k_{SE}$ is the rate for the thermal detrapping of excition from the shallow defect.

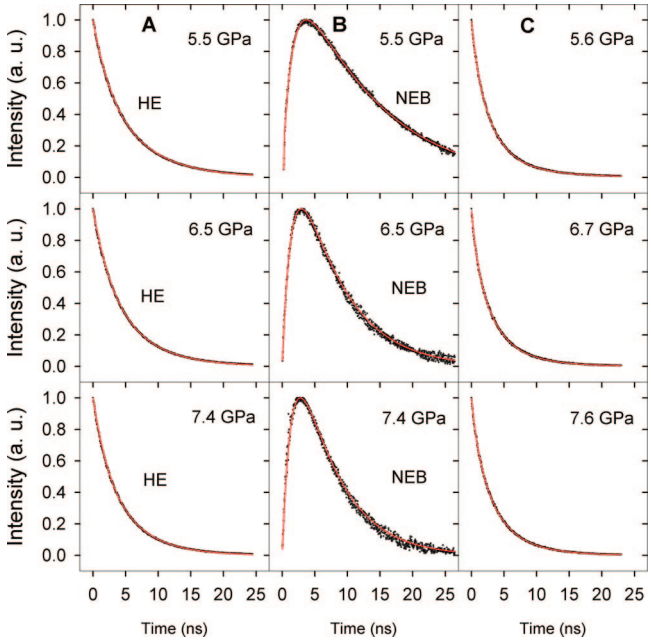


**Figure 10.** Fluorescence decay curves at several nonhydrostatic compressions. Panel A: decay curves at the HE part of the fluorescence spectrum obtained with a 360 nm ($27.8 \times 10^3$ cm$^{-1}$) line excitation: experiment (dots); fitting using eq 1 (solid lines). Panel B: decay curves for the NEB obtained with a 360 nm line excitation (see explanation in text): experiment (dots); fitting using eq 3 (solid lines). Panel C: decay curves upon excitation with a 532 nm ($18.8 \times 10^3$ cm$^{-1}$) line: experiment (dots); fitting using a generic two exponential function (solid lines).

cm$^{-1}$). In this case, the observed emission resulted primarily from the excitation of the new absorption band.

The first set of experiments was designed to determine the nature of the new emission band. Typical time-resolved fluorescence decay curves under hydrostatic (<5 GPa) and nonhydrostatic (>5 GPa) compressions are shown in Figure 8. Several observations are in order: (i) fluorescence decays are not a single exponential, even under hydrostatic compression, (ii) departure from single exponential decay becomes larger at higher pressures, (iii) decay curves are virtually the same for the LE and HE parts of the fluorescence spectra under hydrostatic compression, (iv) fluorescence decay curves change profiles at the onset of nonhydrostaticity, and (v) decay curves measured at the LE part of the spectrum, which corresponds to the new emission band, clearly display an initial increase.

A non-single-exponential decay of fluorescence from chemically pure anthracene crystal is generally associated with the presence of structural defects, e.g., refs 2, 28, and 29. These defects can act as trapping centers for migrating singlet excitons. Significant changes in the fluorescence decay profiles at the onset of nonhydrostaticity indicate changes in the energy migration process. We propose that the observed changes are mainly due to the formation of new structural defects. To obtain further insight into these defects, we analyzed the fluorescence decay curves in terms of a kinetic model for energy migration in organic molecular crystals.[30,31]

In Figure 9, we present a simplified scheme, which was used to describe decay curves under hydrostatic and nonhydrostatic compression. It is assumed that the emission under hydrostatic compression is composed of emission of free excitons and excitons trapped in shallow defects. It is further assumed that under nonhydrostatic compression another component emerges which originates from the emission of excitons from the deep defects. The latter can contribute to the LE band of the emission spectrum. The solution of rate equations for this scheme assumes $\delta$-function laser excitation pulse, time-independent rates, and negligible exciton−exciton interactions. Therefore, the fluorescence decays dependencies for the free anthracene excitons ($I_{EB}$) and for the excitons trapped in shallow ($I_{ST}$) and deep ($I_{DT}$) defects are

$$I_{EB}(t) = C_1[K_1 \exp(-k_1 t) + \exp(-k_2 t)] \quad (1)$$

$$I_{ST}(t) = C_2[\exp(-k_1 t) - \exp(-k_2 t)] \quad (2)$$

$$I_{DT}(t) = C_3\left[\exp(-k_1 t) + \frac{K_2}{K_1}\exp(-k_2 t) - \left(1 + \frac{K_2}{K_1}\right)\exp(-k_3 t)\right] \quad (3)$$

$$k_{1,2} = \frac{1}{2}\{(k_E + k_S) \pm [(k_E - k_S)^2 + 4k_{ES}k_{SE}]^{1/2}\} \quad \text{and} \quad k_3 = k_{DT} \quad (4)$$

where $C_1$, $C_2$, $C_3$ are constants and

$$K_1 = \frac{k_2 - k_E}{k_E - k_1}, \quad K_2 = \frac{k_{DT} - k_1}{k_{DT} - k_2}, \quad k_E = k_{EB} + k_{ES} + k_{ED}, \quad k_S = k_{ST} + k_{SE} \quad (5)$$

All quantities are described in the caption of Figure 9.

A combination of eqs 1 and 2 can be used to describe fluorescence decays under hydrostatic compression. However, because of the regular shape of the florescence spectra and, virtually, the same fluorescence decay curves at different parts of the fluorescence spectra, the decays could be fitted with the use of eq 1 only, indicating an insignificant emission from the shallow defects. For nonhydrostatic compression, eq 1 was used to describe the fluorescence decays detected at the HE part of the fluorescence spectrum, whereas eq 3 was used to describe the fluorescence decay detected from the NEB. This band, unfortunately, overlapped with the tail of the free excitons spectrum. The contribution of the emission from the free excitons to the LE part of the spectrum was evaluated from the fitting of the spectra. The approximated decay curves for the NEBs were then obtained by subtracting the weighted intensity of the decay curve for free excitons from the decay curve measured at the LE of the spectrum. The uncertainty in determination of the intensity contribution from NEB to LE was estimated to be less than 10%.

Examples of the application of eqs 1 and 3 to experimental data are shown in Figures 8 and 10 (panels A and B),

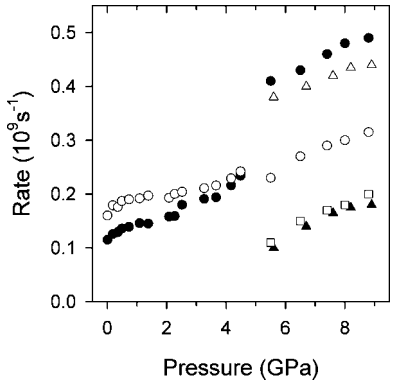


**Figure 11.** Effect of hydrostatic and nonhydrostatic compression on fluorescence rates associated with the model proposed in Figure 9. Combined rates: $k_E$ (solid circles) and $k_S$ (open circles). Decay rate from a deep defect upon excitation with a 360 nm line: $k_D$ (open squares). Decay rates upon excitation of the new absorption band with a 532 nm line: $k_A$ (open triangles) and $k_B$ (solid triangles).

respectively. In all cases, very good fits were attained with a particular set of the emission and transfer rates. Figure 10 (panel C) also includes decay curves obtained with a direct excitation of the new absorption band. In this case, the emission decay curves could be fitted with two exponential components and rates referred to as $k_A$ and $k_B$. The pressure dependencies of some rates obtained from the fitting of decay curves under hydrostatic and nonhydrostatic compression are collected in Figure 11. Several features can be noted in this compilation: (i) a monotonic increase in the $k_E$ and $k_S$ rates under hydrostatic compression, (ii) a significant increase in the $k_E$ rate at the onset of nonhydrostaticity due to occurrence of the excition transfer ($k_{ED}$) to deep defects, (iii) further increase in rates with increasing nonhydrostatic compression, and (iv) similar values and pressure dependencies of the $k_{DT}$ and $k_B$ rates. The last result evidently indicates that the same deep defects are responsible for the new bands in the emission and absorption spectra. The fluorescence lifetime associated with these defects is about 10 ns at 5.5 GPa.

**3.3. Optical Images: Microscopic Nature of Defects.** The changes in the fluorescence and absorption spectra were accompanied by a significant transformation of the crystal color. The optical images of compressed anthracene are presented in Figure 12. These images were obtained on the same sample as the fluorescence spectra shown in Figure 2. Colorless at ambient conditions, the crystal became gradually yellow with increasing hydrostatic compression. Changes in the sample color were fully reversible upon release of the pressure. In contrast, nonhydrostatic compression transformed the crystal color to red, above ~7.0 GPa. In addition to the red color, numerous lines could be noted on the crystal surface. Initially, lines occurred in one direction (at ~5 GPa) and then, additionally, in other directions at higher pressures. A careful examination of several samples revealed a characteristic pattern of crossing lines on the (001) crystal surface (see Figure 13). The measured angles between intersecting lines on several crystals resulted in an average value of 76° with a standard deviation of ±5°. It should be mentioned that the crossing lines remained on the crystal even after the pressure release.

The occurrence of intersecting lines on the crystal surface under nonhydrostatic compression could be linked to structural features in the crystal. Analysis of the structural parameters of anthracene crystal indicates that the angle between the [100] and [110] directions assumes 36.6° at 8 GPa.[15,18] Therefore, the angle between [110] and [1$\bar{1}$0] directions will be 73.2°, as

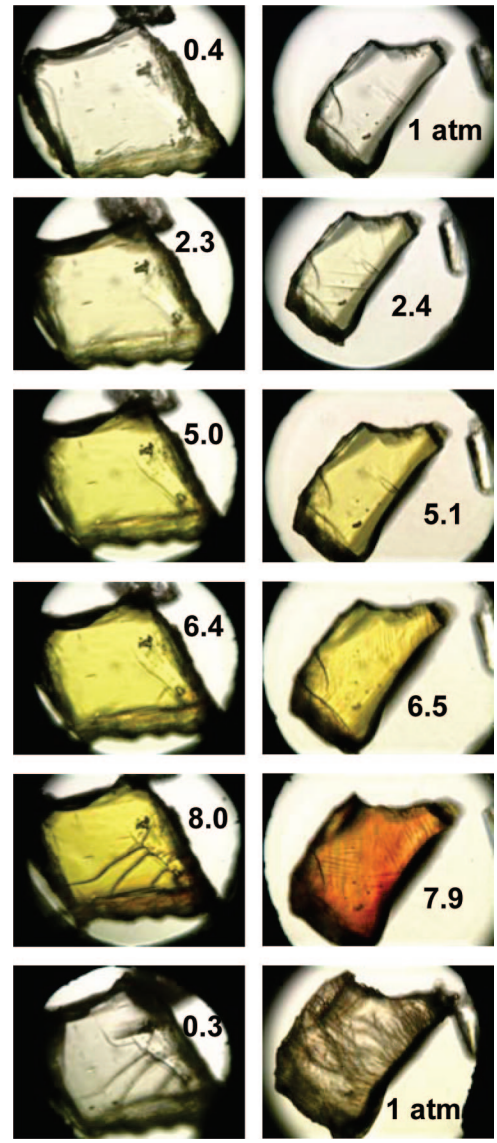


**Figure 12.** Optical images of anthracene single crystal at several pressures. Left panel represents hydrostatic compression, and right panel represents nonhydrostatic compression. The bottom images represent the sample upon release of the pressure. The numbers on the images represent pressures in GPa. The aperture in the gasket was ~0.2 mm.

illustrated in Figure 14. This value is in good agreement with the measured angle in our experiments. This similarity implies that nonhydrostatic compression[32] imposed on the crystal causes plastic changes on the (001) plane along the [110] and [1$\bar{1}$0] directions. But, it would require that the (110) [1$\bar{1}$0] and (1$\bar{1}$0) [110] slip systems be operative in the crystal. Indeed, these two complementary slip systems were suggested to be the key to the initiation of photodimerization on the (001) surface of anthracene.[33] It was also found that for these slips to occur, an incipient presence of stacking faults along the [110] or [1$\bar{1}$0] direction was needed. Actually, the experiments using transmission electron microscopy revealed dislocation faults along [110] direction in solution-grown anthracene crystals.[34] On the basis of these correlations, we propose that nonhydrostaticity introduces plastic deformation in the form of dislocations along [110] and [1$\bar{1}$0] directions on the (001) surface. The relationship between these dislocations and the observed changes in the electronic structure is discussed next.

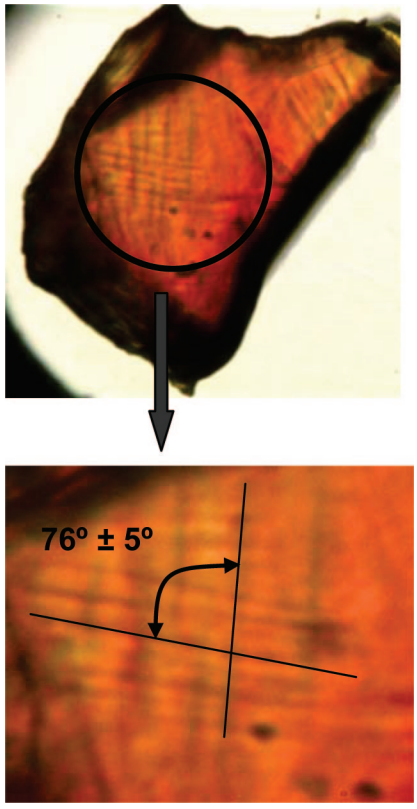


**Figure 13.** Optical images showing the intersecting lines on the (001) plane of anthracene crystal under nonhydrostatic compression. The indicated angle is the average value from measurements on several crystals.

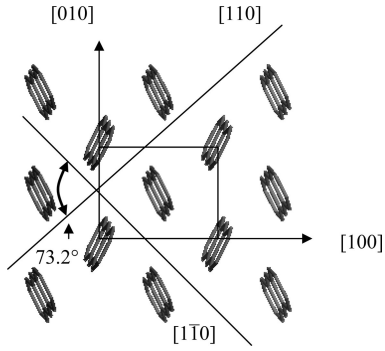


**Figure 14.** Projection of anthracene structure on the (001) plane. The angle between the [110] and [1$\bar{1}$0] directions was calculated at 8 GPa for the unit cell parameters from ref 18.

**3.4. Origin of Changes in the Electronic Structure.** Three main features were observed in the absorption and fluorescence of anthracene crystal at the onset of nonhydrostaticity: (i) a new band at the shoulder of absorption edge, (ii) a new low-energy band in the fluorescence spectra located ~18.4 × $10^3$ $cm^{-1}$ (at 5.1 GPa), and (iii) changes in the decay fluorescence profiles at the low-energy part of the fluorescence spectra. These features can be linked to plastic deformation observed in the crystal. As shown above, the plastic changes have been related to structural defects observed through both electronic and optical measurements. Also, we have indicated that these defects occur in the form of dislocation planes activated by inhomogeneous stresses. In particular, we have suggested that the (110) [1$\bar{1}$0] and (1$\bar{1}$0) [110] slip systems can lead to the formation of the observed [110] and [1$\bar{1}$0] dislocations on the (001) surface of the anthracene crystal. The effect of [110] dislocation on the anthracene microstructure is illustrated in Figure 15. As can be

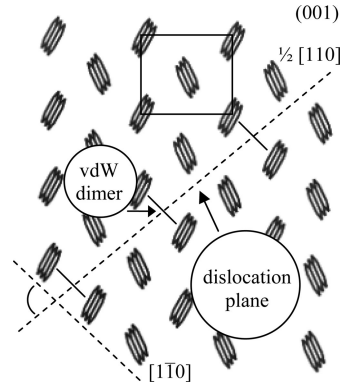


**Figure 15.** Diagrammatic representation of anthracene (001) plane. Illustration of the van der Waals (vdW) dimer sites formation along [110] dislocations.

seen, the 1/2 [110] partial dislocation can lead to the formation of parallel arrangements between two anthracene molecules across the dislocation plane. This arrangement is very similar to the structures found in crystals with dimeric and excimeric properties, for instance, in pyrene and α-perylene. The stability of van der Waals (vdW) dimeric structures in these crystals is mainly linked to a short distance of 0.35 nm between two parallel molecules. In the case of anthracene, if one assumes that the perfect crystal geometry is maintained during dislocation formation, the distance between two adjacent molecules would be ~0.46 nm, at 8 GPa. However, we believe that the actual distance will be smaller due to deformation of the crystal under nonhydrostatic compression, thus allowing for the formation of vdW dimers.

Typically, vdW dimeric structures from aromatic molecules are unbound in the ground state.[1] However, recent studies of aromatic vdW clusters demonstrated that two isomers in anthracene clusters (dimers) can exist in the ground state with a parallel-displaced molecular geometry.[35,36] The parallel-displaced configuration in anthracene clusters appears very similar to that proposed under nonhydrostatic compression. Therefore, we postulate that dimeric structures produced in compressed anthracene have stable ground states as indicated by the formation of the new absorption band. The stabilization of these structures may result from pressure-enhanced differences in intermolecular interaction near the dimers (local defects) compared to regions far away from dimeric sites.

The association of dimeric structures with observed features in the fluorescence spectra and fluorescence decays can be explained as follows. In the case of UV excitation (337 or 360 nm lines), the light is absorbed in the "perfect" crystal region with the formation of exciton. Subsequently, the exciton can either fluoresce or migrate to be eventually trapped in the dimeric defect. The resulting emission from the defect has a broad and structureless spectrum, demonstrating the excimeric character of the emitting state. The observed lifetime of this emission at 5.5 GPa is ~10 ns. It is a significantly shorter lifetime than that of the anthracene excimer emission observed previously in hydrocarbon matrixes (225 ns)[37] and in helium jets (300 or 15 ns, depending on the type of excimer).[35,38] The shorter lifetime in our experiments may indicate a large nonradiative rate of excimeric emission. It might be due to the enhanced coupling between the ground and excited state of dimeric defect as a result of high pressure.

In the case of excitation with the 532 nm (18.8 × $10^3$ $cm^{-1}$) line, which is within the absorption of dimer, the excitation leads directly to occupation of the excited dimer state rather than the

excimer state. Because the excited states of the vdW dimer are easily coupled to the lower-lying excimer states,[35] the observed broad and structureless fluorescence spectrum may be a combination of emissions from both the excited vdW dimer and the excimer. This possibility is consistent with the observed two-component emission decay. The longer lifetime (~10 ns) would correspond to the excimer emission and the shorter (~3 ns) to the dimer emission. The longer lifetime matches exactly the value obtained for the excimer emission upon indirect excitation of the dimeric defect. Therefore, it confirms that the observed changes in the electronic spectra are associated with the dimeric defects formed under nonhydrostatic compression.

## 4. Concluding Remarks

By subjecting anthracene single crystals to hydrostatic and nonhydrostatic stresses, we have examined the role of nonhydrostaticity on changes in electronic and optical properties under static compression. Several new features were observed in the electronic spectra at the onset of nonhydrostatic compression including new bands in the emission and absorption spectra. These changes were linked to plastic deformation in the crystal and the formation of dislocations. In particular, we provided evidence that dislocations along [110] and [1$\bar{1}$0] directions, especially the partial ones, in the (001) plane are responsible for the observed spectral features. Such dislocations can lead to the formation of dimeric sites which can facilitate the formation of stable dimers and excimers. Both these species are associated with the formation of new bands in the electronic spectra. Specifically, we demonstrated that nonhydrostatic compression caused the following: (i) a stable electronic ground state of dimeric species was formed and (ii) the excimer-like emission was observed that had a lifetime of 10 ns.

Although we were not able to quantify the detailed stress state imposed on the crystal, we showed that the presence of nonhydrostatic stresses can change the molecular crystal response significantly. Therefore, in studies of molecular crystals under high pressure, some of the observed effects might not be related to pressure, but rather to stress deviators, and, consequently, to crystal deformation. Also, studies under intentionally introduced nonhydrostaticity, as was done here, can provide further insight into processes occurring under shock compression where nonhydrostatic conditions are the norm.[39]

**Acknowledgment.** This work was supported by ONR MURI Grants N00014-01-1-0802 and N00014-06-1-0459 and DOE Grant DEFG0397SF21388. The TCSP measurements were performed in the Environmental Molecular Sciences Laboratory, a National Scientific User Facility sponsored by the Department of Energy's Office of Biological and Environmental Research and located at Pacific Northwest National Laboratory.

## References and Notes

(1) Pope, M.; Swenberg, Ch. E. *Electronic Processes in Organic Crystals and Polymers*; Oxford University Press: New York, 1999.

(2) Silinsh, E. A.; Capek, V. *Organic Molecular Crystals: Interaction, Localization, and Transport Phenomena*; Springer-Verlag: Berlin, Heidelberg, New York, 2000.

(3) Karl, N. In *Crystals: Growth, Properties, and Applications*; Freyhardt, H. C., Ed.; Springer-Verlag: Berlin, Heidelberg, New York, 1980; Chapter 1.

(4) Wiederhorn, S.; Drickamer, H. G. *J. Phys. Chem. Solids* **1959**, *9*, 330.

(5) Jones, P. F.; Nicol, M. *J. Chem. Phys.* **1965**, *43*, 3759.

(6) Offen, H. W. *J. Chem. Phys.* **1966**, *44*, 699.

(7) Ohigashi, H.; Shirotani, I.; Inokuchi, H.; Minomura, S. *Mol. Cryst.* **1966**, *1*, 463.

(8) Jones, P. F.; Nicol, M. *J. Chem. Phys.* **1968**, *48*, 5440.

(9) Okamoto, B. Y.; Drickamer, H. D. *J. Chem. Phys.* **1974**, *61*, 2870.

(10) Nicol, M.; Vernon, M.; Woo, J. T. *J. Chem. Phys.* **1975**, *63*, 1992.

(11) Otto, A.; Keller, R.; Rahman, A. *Chem. Phys. Lett.* **1977**, *49*, 145.

(12) Mizuno, K.; Matsui, A. *J. Phys. Soc. Jpn.* **1986**, *55*, 2427.

(13) Dreger, Z. A.; Lucas, H.; Gupta, Y. M. *J. Phys. Chem. B* **2003**, *107*, 9268.

(14) Leger, J. M.; Aloualiti, H. *Solid State Commun.* **1991**, *79*, 901.

(15) Oehzelt, M.; Resel, R.; Nakayama, A. *Phys. Rev. B* **2002**, *66*, 174104.

(16) Oehzelt, M.; Weinmeier, K.; Heimel, G.; Puschnig, P.; Resel, R.; Ambrosch-Draxl, C.; Porsch, F.; Nakayama, A. *High Pressure Res.* **2002**, *22*, 343.

(17) Oehzelt, M.; Heimel, G.; Resel, R.; Puschnig, P.; Hummer, K.; Ambrosch-Draxl, C.; Takemura, K.; Nakayama, A. *J. Chem. Phys.* **2003**, *119*, 1078.

(18) Hummer, K.; Puschnig, P.; Ambrosch-Draxl, C. *Phys. Rev. B* **2003**, *67*, 184105.

(19) Resel, R.; Oehzelt, M.; Shimizu, K.; Nakayama, A.; Takemura, K. *Solid State Commun.* **2004**, *129*, 103.

(20) Adams, D. M.; Tan, T. K. *J. Chem. Soc., Faraday Trans. 2* **1981**, 1711.

(21) Zhao, L.; Baer, B. J.; Chronister, E. L. *J. Phys. Chem. A* **1999**, *103*, 1728.

(22) Gupta, Y. M.; Shen, X. A. *Appl. Phys. Lett.* **1991**, *58*, 583.

(23) Sharma, S. M.; Gupta, Y. M. *Phys. Rev. B* **1991**, *43*, 879.

(24) Shen, X. A.; Gupta, Y. M. *Phys. Rev. B* **1993**, *48*, 2929.

(25) Dreger, Z. A.; Yang, G.; White, J. O.; Li, Y.; Drickamer, H. G. *J. Phys. Chem. A* **1997**, *101*, 9511.

(26) Holtom, G. R. *Proc. SPIE.* **1990**, *1204*, 2.

(27) Offen, H. W. In *Organic Molecular Photophysics*; Birks, J. B., Ed.; John Wiley & Sons: London, New York, Toronto, Sydney, 1973; Vol. 1, Chapter 3.

(28) Ostapenko, N. I.; Sugakov, V. I.; Shpak, M. T. *Spectroscopy of Defects in Organic Crystals*; Kluwer Academic Press: Dordrecht, Boston, London, 1993.

(29) Galanin, M. D.; Khan-Magometova, S. D.; Chizhikova, Z. A. *J. Lumin.* **1975**, *9*, 459.

(30) Powell, R. C.; Soos, Z. G. *Phys. Rev.* **1972**, *5*, 1547.

(31) Braun, A.; Pfisterer, H.; Schmid, D. *J. Lumin.* **1978**, *17*, 15.

(32) In this study, we were not able to determine the exact stress state imposed on the nonhydrostaticaly compressed crystal. The mean stress was used as determined from the position of the $R_2$ ruby line.

(33) Crisp, G. M.; Walmsley, S. H. *Chem. Phys.* **1982**, *68*, 213.

(34) Parkinson, G. M.; Thomas, J. M.; Goringe, M. J.; Smith, D. A. *Chem. Phys. Lett.* **1979**, *63*, 436.

(35) Matsuoka, T.; Kosugi, K.; Hino, K.; Nishiguchi, M.; Ohashi, K.; Nishi, N.; Sekiya, H. *J. Phys. Chem. A* **1998**, *102*, 7598.

(36) Gonzalez, C.; Lim, E. C. *Chem. Phys. Lett.* **2000**, *322*, 382.

(37) Fielding, P. E.; Jarnagin, R. C. *J. Chem. Phys.* **1966**, *47*, 247.

(38) The shorter lifetime was reported for the sandwich conformation of two anthracene molecules with long molecular axes parallel and short axes at 55° to one another.

(39) Hemmi, N.; Dreger, Z. A.; Gupta, Y. M. *J. Phys. Chem C* **2008**, *112*, 7761.

JP808247K